On the Effect of Constraint Enforcement on the Quality of Numerical Solutions in General Relativity

Florian Siebel
Max-Planck-Institut für Astrophysik
Karl-Schwarzschild-Str. 1
85741 Garching, Germany
florian@mpa-garching.mpg.de

Peter Hübner
Linienstraße 45a
82041 Oberhaching,
Germany
pth@epost.de

In Brodbeck et al 1999 [1] it has been shown that the linearised time evolution equations of general relativity can be extended to a system whose solutions asymptotically approach solutions of the constraints.
In this paper we extend the non-linear equations in similar ways and investigate the effect of various possibilities by numerical means. Although we were not able to make the constraint submanifold an attractor for all solutions of the extended system, we were able to significantly reduce the growth of the numerical violation of the constraints. Contrary to our expectations this improvement did not imply a numerical solution closer to the exact solution, and therefore did not improve the quality of the numerical solution.

I. INTRODUCTION

Many physical theories are based upon systems of partial differential equations which contain more equations than variables like Maxwell's equations or general relativity. The initial data for the time evolution equations cannot be given freely, they must satisfy constraints. It is necessary for the consistency of the theory, that for any data of the time evolution equations which initially satisfy the constraints, the constraints are satisfied for all times. This property is called "propagation of constraints".
Let us consider Maxwell's equations in vacuum as a simple example. The time evolution equations tell us that the time derivative of the electric and magnetic field are proportional to the curl of the magnetic and electric field. The vanishing of the divergence of the electric and magnetic field are the constraints. It can easily be shown that the constraints propagate.
In cases where the solutions of a system of partial differential equations are determined by numerical means we cannot expect to get an exact propagation of the constraints. Due to the

discretisation of the equations the numerical solution deviates from the exact solution by the discretisation error. As a consequence, the constraints are not fulfilled exactly after having evolved for some time, even if the initial data solved the constraints. In the spirit of [2] we call a discretisation of the time evolution equations compatible with the constraints, if the numerical violation of the constraints has the same convergence order as the discretisation of the time evolution equations. Unfortunately the experience of numerical relativity shows that compatibility is not sufficient for obtaining numerical solutions with small numerical violations of the constraints. In many cases the violation of the constraints seems to grow at least exponentially with time. This effect is believed to be a major contribution to the numerical error of numerically calculated solutions.

In this work we examine the effect of changing the evolution equations outside the submanifold of data on which the constraints are satisfied. Although our method is different, we should mention that already in [3] such a change has been suggested. Furthermore, to our knowledge, we perform the first systematic analysis of the correlation between the violation of the constraints and the quality of numerical solutions in general relativity.

As the solutions of the field equations of general relativity satisfy the constraint equations for all times, the solutions are not affected by modifications of the evolution equations for data which do not satisfy the constraints. Let us denote the subspace of the function space of solutions to the evolution equations which satisfy the constraints as "constraint submanifold". In [1] it has been proven, that at least for the linearised Einstein equations the constraint submanifold can be made an attractor for the linearised time evolution equations.

If the solution of the evolution equations automatically approaches the constraint submanifold, the system of evolution equations carries a dissipative term in it, and therefore, the numerical solution will also approach the constraint submanifold provided the grid is not too coarse. Therefore, to avoid a numerical violation of the constraints, it is sufficient to make the constraint submanifold an attractor of the (modified) evolution equations. In such a case the constraint submanifold is 'asymptotically stable'.

In Brodbeck et al. [1] a general method has been proposed to derive symmetric hyperbolic extensions of symmetric hyperbolic evolution equations with first order constraints which are promising candidates for asymptotic stability. These extended systems are called λ-systems. In the same article it has also been proven, that at least in the case of the linearised Einstein equations there exist parameters such that the constraint submanifold is indeed an attractor for the modified evolution equations.

As the extension of the analysis to the non-linear Einstein equations seemed to be beyond the scope of present analytical techniques, we took a numerical approach in this paper and investigated the following questions: Firstly, can we, simply by way of numerical experiments, find a λ-system for the non-linear Einstein equations for which the constraint submanifold is attractive? And secondly, is the numerical solution of the modified systems closer to the exact solution than the numerical solution of the unmodified system? To reduce the complexity and to have exact solutions available to compare with, we have restricted our investigations to solutions with two Killing vectors.

In our experiments we were able to find a variety of λ-systems for which the violation of all constraints is improved. However, we did not find a single system for which the constraint submanifold is asymptotically stable. Surprisingly, the improvement in the constraint violation did not imply an improvement of the numerical solution.

This paper is structured as follows: In chapter II we introduce parametrised λ-systems and describe the simplifications implied by the symmetry assumptions. In the next chapter we sketch the numerical implementation, recall important features of the exact solutions used in the comparisons, and define the measures used for quality assessments. Chapter IV contains the actual numerical investigations, where we describe the performed probing of the parameter space. Using selected examples we demonstrate the influence of the individual parameters on the quality of the numerical solution.

II. THE PARAMETRISATION OF THE λ-SYSTEM

The construction of a λ-system is based on a split of the system of equations into symmetric hyperbolic evolution equations and first order constraints [1]. There are various possibilities to write Einstein's equations in a form like this.
In our work, we take the conformal field equations [4, 5, 6] in the first-order formulation described in [7]. Looking at the equations (13) and (14) of [7], it is easy to see that Einstein's equations and their extension, the conformal field equations, are a "quasilinear version" of Maxwell's equations. We use the conformal field equations instead of Einstein's equations to obtain an easy and well defined treatment of grid boundaries, as discussed in [7]. Since we are primarily interested in the effect of the non-linearities, we can reduce the computational complexity by restricting ourselves to asymptotically A3 spacetimes [8], which are spacetimes with two commuting, hypersurface orthogonal Killing vector fields. We align the y and z coordinates with the Killing orbits. Our solutions do therefore not depend on the spacelike coordinates y and z. Under these symmetry assumptions, the conformal field equations can be written in the following form

$$\tilde{\mathbf{A}}\frac{\partial}{\partial t}g + \mathbf{A}\frac{\partial}{\partial x}g - b_g = 0 \tag{1a}$$

$$\frac{\partial}{\partial t}f - b_f = 0 \tag{1b}$$

$$\frac{\partial}{\partial x}f - c_f = 0, \tag{1c}$$

with a time coordinate t labelling the spacelike hypersurfaces, x being the non-Killing spacelike coordinate, and

$$g = (k_{11}, {\gamma^1}_{11}, E_{22}, E_{33}, B_{23}, {}^{(0,1)}\hat{R}_1, {}^{(1,1)}\hat{R}_{11}) \tag{2a}$$

$$f = (h_{11}, h_{22}, h_{33}, k_{22}, k_{33}, {\gamma^1}_{22}, {\gamma^1}_{33}, E_{11}, {}^{(1,1)}\hat{R}_{22}, {}^{(1,1)}\hat{R}_{33}, \Omega, \Omega_0, \Omega_1, \omega). \tag{2b}$$

The tensor h_{ab} is the 3-metric, k_{ab} the extrinsic curvature of the spacelike hypersurfaces, ${\gamma^a}_{bc}$ the connection for h_{ab}, ${}^{(0,1)}\hat{R}_a$ and ${}^{(1,1)}\hat{R}_{ab}$ parts of the tracefree part of the Ricci tensor, E_{ab} and B_{ab} the electric and magnetic part of the conformal Weyl tensor, Ω the conformal factor, Ω_0 and Ω_1 its normal and space derivative, and ω a second derivative of the conformal factor, as described in more detail in [7]. The symmetric matrices $\tilde{\mathbf{A}}$, $\mathbf{A}$ and the vectors b_g, b_f and c_f depend on g, f and gauge functions. The matrix $\tilde{\mathbf{A}}$ is positive definite, hence the system consisting of the equations (1a) and (1b) is symmetric hyperbolic.

The variables, which are functions of t and x only, have been split into two classes, called g and f. For the variables denoted by f the system contains evolution equations and constraints. Since there are only evolution equations for the variables g, these represent the degrees of freedom.

When we evolve initial data forward in time by means of the evolution equations (1a) and (1b), the constraints (1c) fulfil an evolution equation from which the propagation of the constraints can be derived.

In the following we will call (1a) and (1b) the 'unextended system'. To obtain the new, extended system, the λ-system, additional variables, called λ, are introduced and the constraint equations are extended to evolution equations for the new variables:

$$\tilde{\mathbf{A}}\frac{\partial}{\partial t}g + \quad \mathbf{A}\frac{\partial}{\partial x}g - \quad b_g + \mathbf{C}\lambda = 0 \tag{3a}$$

$$\frac{\partial}{\partial t}f + \quad \mathbf{B}\frac{\partial}{\partial x}\lambda - \quad b_f + \mathbf{D}\lambda = 0 \tag{3b}$$

$$\frac{\partial}{\partial t}\lambda + \ \mathbf{B}^T\frac{\partial}{\partial x}f - \mathbf{B}^T c_f + \mathbf{E}\lambda = 0. \tag{3c}$$

The quantities $\mathbf{B}, \mathbf{C}, \mathbf{D}$, and $\mathbf{E}$ are matrices. $\mathbf{B}^T$ denotes the transposed matrix of $\mathbf{B}$. This system is constructed in such a way that

1. it is symmetric hyperbolic.

2. in the case in which the variables λ vanish identically the system is reduced to the original system (1).

Due to the second requirement, the λ-system is a generalisation of the original system. The first requirement implies well-posedness of the initial value problem. Apart from the restrictions resulting from the two conditions above, the choice of the parameters $\mathbf{B}, \mathbf{C}, \mathbf{D}$, and $\mathbf{E}$ is free. It is the aim to choose them in such a way that for all solutions of the system the variables λ decay, which then implies that the solution is driven towards a solution of the constraints.

We will now shortly explain why we have introduced these parameters. Let us assume that the constraint equations are not fulfilled exactly, i.e. $\partial_x f - c_f \neq 0$, and $\lambda = 0$ initially. In the case of vanishing $\mathbf{E}$, the variables λ are the time integral of the violation of constraints - as a result of the new evolution equation (3c). For non-vanishing $\mathbf{E}$, in addition, the $\mathbf{E}\lambda$-term will have a damping or amplifying effect onto the variables λ, depending on the eigenvalues of $\mathbf{E}$. For positive eigenvalues we expect damping, for negative eigenvalues amplification. The information about the violation of constraints, saved in the variables λ, is coupled back to the variables (g, f) by the terms $\mathbf{B}\partial_x\lambda$, $\mathbf{D}\lambda$, and $\mathbf{C}\lambda$.

III. THE NUMERICAL IMPLEMENTATION

In this section we will describe the basic elements of the numerical implementation which we use to compare the quality of solutions obtained by solving the λ-system with the quality of solutions obtained by solving the unextended system. These elements are the construction

of initial data, the scheme to numerically integrate the time evolution equations, and the measures used to assess the quality of our numerical solutions. In addition we will briefly describe the exact solutions which we used as reference solutions.

A Constructing hyperboloidal initial data

In order to analyse the numerical behaviour of the λ-system, we first have to construct initial data for the conformal field equations. These data are called hyperboloidal initial data.
In [9, section 2] the procedure of calculating initial data has been described in detail for the case without any symmetry assumptions. We slightly modified the procedure by making use of the symmetry assumptions, namely that our spatial grid is only one-dimensional (1D). For an exact solution we prescribe the 4-metric g_{ab} and the conformal factor Ω as functions of (t, x). From those we calculate our variables (g, f) and the gauge source functions numerically. The code has also got the functionality to perform a coordinate transformation to express the exact solution in new coordinates (t', x').
In the calculations presented in this paper we used $\lambda = 0$ as initial setting for λ.

B The integration of the time evolution equations

In order to discretise the evolution equation

$$\partial_t \mathbf{u} + \underline{\underline{A}}(\mathbf{u})\ \partial_x \mathbf{u} = \underline{b}(\mathbf{u}) \tag{4}$$

for the vector of variables $\mathbf{u}$, we adjust the second-order scheme described in [9, section 3.1] to our symmetry assumption, i.e. we perform a Strang splitting ansatz to split equation (4) into a principal part

$$\partial_t \mathbf{u} + \underline{\underline{A}}(\mathbf{u})\ \partial_x \mathbf{u} = 0 \tag{5}$$

and a source part

$$\partial_t \mathbf{u} = \underline{b}(\mathbf{u}). \tag{6}$$

We then solve the principal part (5) by the rotated Richtmyer scheme. With one spatial dimension, this is equivalent to the standard second-order Lax-Wendroff method [10]. The source part is integrated by the pseudo-implicit Heun-scheme. As described in [9], principal and source part are combined in different order, depending on whether the time step is odd or even, to achieve second-order convergence.

In [9] it was shown how superior a 4th order scheme would be. In a normal application this superiority would be a big advantage — here it is a disadvantage, however: We are going to analyse the impact of a drift away from the constraint submanifold on the quality of the solution. This drift originates in the discretisation error. If the scheme is very accurate, the drift is very small, too. But then, the differences in the quality of the numerical solutions are also very small, which makes it harder to distinguish between them. This explains why we use the second-order scheme.

In the runs described in part IV we cover the spacelike hypersurface with 161 grid points. The length of the time step is chosen dynamically by evaluating the Courant-Friedrichs-Lewy condition for each time slice. If not explicitly stated otherwise, we use half of what would be allowed by the Courant-Friedrichs-Lewy condition.

C Measures of quality

We use the following measures to analyse the quality of a numerical solution.
Firstly, we determine the numerical violation of the constraints as a measure of the distance from the constraint submanifold. To be able to present our findings with a limited number of plots we condense the information by using the "norm"

$$||\Delta_{\mathcal{C}}||(t) := \sqrt{\sum_l \int_{\Omega>0} \mathcal{C}_l(t,x)^2 dx}, \tag{7}$$

where the summation includes all constraints $\mathcal{C}_l(t,x)$. In the actual numerical calculations the integral is of course replaced by a sum over all grid points with $\Omega > 0$, which represent physical spacetime. In the conformal approach to numerical relativity grid points with $\Omega < 0$ represent a formal extension of the grid without physical relevance. Therefore, it would be wrong to include them into the measure.
Secondly, we compare our numerical solution to the exact solution. Since the numerical calculation of $({}^{(1,1)}\hat{R}_{ab}, E_{ab}, B_{ab})$ from the given solution (g_{ab}, Ω) involves solving elliptic equations (cf. [9]), we compare $(\Omega\, {}^{(1,1)}\hat{R}_{ab}, \Omega^2 E_{ab}, \Omega B_{ab})$ to the corresponding quantities from the exact solution and call the result "pseudodifference" $\mathcal{P}_l(t,x)$. In [9] it was found that with respect to the relative error this is equivalent to the difference in the variables. Again, to be able to present our findings with a limited number of plots, we condense the information by using the "norm"

$$||\Delta_{\mathcal{P}}||(t) := \sqrt{\sum_l \int_{\Omega>0} \mathcal{P}_l(t,x)^2 dx}, \tag{8}$$

where the summation includes the variables in the tuple (g, f), but does not include the variables λ.

D The exact solutions used in the numerical experiments

Only a few exact solutions of Einstein's vacuum equations possess both, high symmetries and time dependence, or even better gravitational radiation. The asymptotically A3 solutions do. They can be written as

$$g = \frac{4\sqrt{2}}{\sqrt{t^2+x^2}} e^M(-dt^2+dx^2) + \frac{1}{2}(t^2+x^2)(e^W dy^2 + e^{-W} dz^2) \tag{9a}$$

$$\Omega = \frac{1}{4}(t^2-x^2), \tag{9b}$$

where the functions $M(t,x)$ and $W(t,x)$ are solutions of certain differential equations (cf. [8]). We restricted our analysis to two cases, $M \equiv 0$ and $W \equiv 0$, the A3 solution on the one hand, and $M = -\frac{1}{256}(t^2+x^2)^2$ and $W = \frac{1}{8}(t^2-x^2)$ on the other hand. The second case, unlike the first one, contains gravitational radiation. Both solutions behaved very similarly in our numerical experiments. The amount of gravitational wave content does not seem to be significant for the drift away from the constraint submanifold. For shortness we only present calculations done with the A3 solution.
The solutions given in (9) are already extended beyond the two null-infinities $\mathcal{J}_1$ and $\mathcal{J}_2$ at $t = -x$ and $t = +x$, the shaded region in FIG. 1 shows the physical part. In this repre-

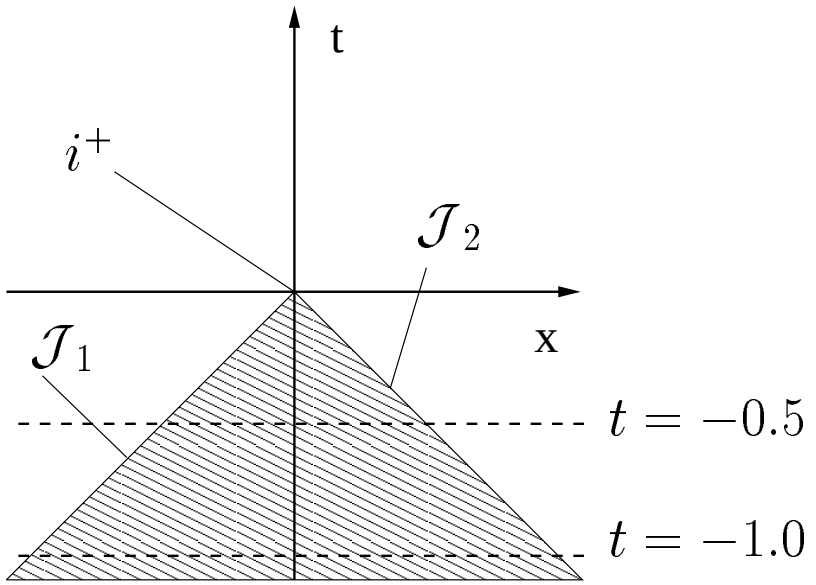

FIG. 1: Conformal diagram of an asymptotically A3 solution. The shaded region corresponds to the physical spacetime.

sentation the point $(0,0)$ represents future time-like infinity i^+. The metric and curvature quantities diverge there. When approaching this point in our numerical evolution, the absolute value of several quantities must increase strongly, which implies increasing absolute errors. However, we confirmed that, even when approaching i^+, our numerical scheme is second-order convergent, the difference between the numerical and the exact solution as well as the violation of constraints converges with a convergence rate of two. In the numerical experiments we start our calculation at $t = -1$ and stop at $t = -1/2$.
In other coordinates FIG. 1 looks different, e.g. one can choose the coordinates such that the $\mathcal{J}$s are at constant x' values and that i^+ lies at a conformal time $t' = \infty$. Since our findings are not influenced by this change of coordinates we refrain from a presentation.

IV. THE QUALITY OF THE NUMERICAL SOLUTION: PARAMETER STUDY

In this section we discuss the effect of the various parameters in the λ-system (3). In the case of the 1D conformal field equations, the matrices $\mathbf{B}, \mathbf{C}, \mathbf{D}$ and $\mathbf{E}$ take values in $\mathbf{R}^{14,14}$, $\mathbf{R}^{7,14}$, $\mathbf{R}^{14,14}$, and $\mathbf{R}^{14,14}$. Since the parameter space is infinite, we had to restrict ourselves to exemplary cases, an exhaustive study by numerical means is impossible.

A Overview

Before going into detail, we discuss the main result of our numerical experiments. Although we were not able to find a suitable choice of parameters such that the constraint submanifold became an attractor for all times, we were able to improve the violation of constraints up to a factor 5 compared to a numerical evolution of the unextended system. There are strong numerical indications that this improvement is obtained at the cost of a solution which is worse with respect to the pseudodifference norm. As an example, the dashed lines in FIG. 2 and 3 show the norms for the violation of constraints (7) and the pseudodifference (8) for a choice of parameters $\mathbf{B} = 3 \cdot \underline{\underline{1}}$, $\mathbf{C} = 0$, $\mathbf{D} = 0$, and $\mathbf{E} = \underline{\underline{1}}$ in the λ-system (by $\underline{\underline{1}}$ we denote the 14×14 unit matrix). The solid lines show the corresponding results for an evolution of the unextended system (1). FIG. 2 shows that the λ-system initially attracts towards the constraint submanifold (until $t = -0.85$), before the violation increases with time. FIG. 3 shows that the pseudodifference norm at the same time increases more rapidly right from the beginning than in the numerical solution of the unextended system.

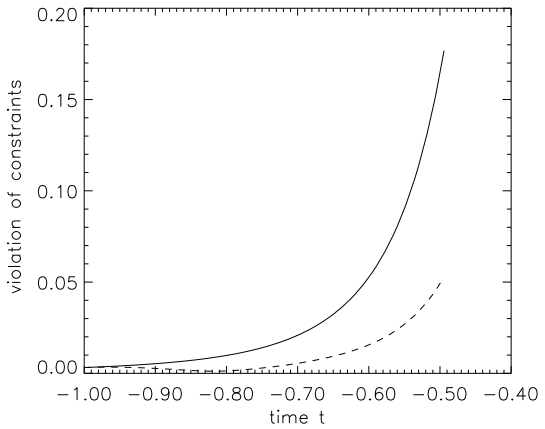

FIG. 2: Constraint norm $||\Delta_{\mathcal{C}}||(t)$ for the λ-system of run 7 (dashed line) in comparison to the unextended system (solid line).

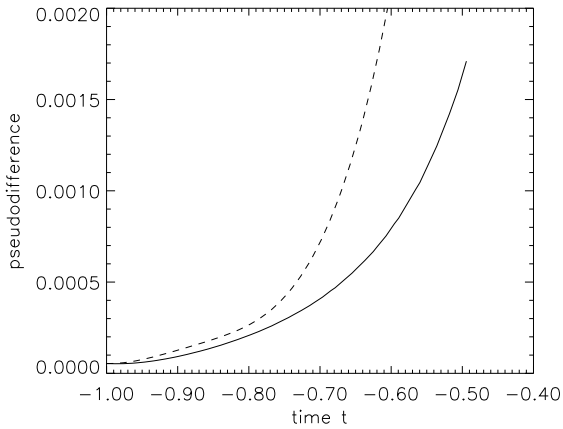

FIG. 3: Pseudodifference norm $||\Delta_{\mathcal{P}}||(t)$ for the λ-system of run 7 (dashed line) in comparison to the unextended system (solid line).

In TABLE 1, we present a summary of the performed numerical experiments. The numbers in the parameter columns denote the value of the diagonal elements of the corresponding diagonal matrix. In the cases in which we studied a range of diagonal elements, we condense

no of run	parameter B	C$^{\alpha)}$	D	E	norm $\|\|\Delta_{\mathcal{C}}\|\|$	$\|\|\Delta_{\mathcal{P}}\|\|$
1	1	$(1,0)$	1	1	$-$	$\uparrow$
2	1	$(1,0)$	$1_{\lambda^2}{}^{\beta)}$	$1_{\lambda^2}{}^{\beta)}$	$-$	$\uparrow$
3	1	$(1,0)$	1	$1_{\lambda^2}{}^{\beta)}$	$-$	$\uparrow$
4	1	$(1,0)$	$1_{\lambda^2}{}^{\beta)}$	1	$-$	$\uparrow$
5	$\|b\| \in]0,1]$	$(0,0)$	0	1	$-$	$\uparrow$
6	1.2	$(0,0)$	0	1	$-$	$\uparrow$
7	3	$(0,0)$	0	1	$-$	$+$
8	1	$(0,0)$	0	10	$+$	$+$
9	1	$(0,0)$	0	$e \in [-1,1]$	$-$	$\uparrow$
10	1	$(0,0)$	0	-3	$-$	$-$
11	1	$(0,0)$	0	-10	$\uparrow$	$+$
12	1	$(0,0)$	0	$(\mathbf{E})_{11} = (\mathbf{E})_{88} = -3^{\gamma)}$	$-$	$-$
13	1	$(0,0)$	0	$(\mathbf{E})_{11} = -3^{\gamma)}$	$-$	$\uparrow$
14	1	$(0,0)$	0	$(\mathbf{E})_{88} = -3^{\gamma)}$	$-$	$\uparrow$
15	1	$(0,0)$	$\|d\| \in [3,15]$	0	$-$	$+$
16	1	$(\pm c, 0)$, $c = 5$	0	0	$-$	$+$
17	1	$(0,0)$	± 10	-3	$-$	$+$
18	1	$(0,0)$	10	1	$-$	$\downarrow$
19	1	$(0,0)$	$5 \cdot \underline{\underline{x}}^{\delta)}$	1	$-$	$+$

α) $\mathbf{C} = (C_1, C_2) \in \mathbf{R}^{7,14}$, where $C_1, C_2 \in \mathbf{R}^{7,7}$.

β) 1_{λ^2} denotes a diagonal matrix with $1 + \lambda_i^2$ at (i,i).

γ) all other elements vanish.

δ) $\underline{\underline{x}}$ denotes a diagonal matrix with space depending diagonal elements.

TABLE I: Results of the numerical experiments for various λ-systems. A number in the column parameter denotes a diagonal matrix with the number on the diagonal. For the notation used in the column norm, please refer to the text.

by combining to parameter intervals with similar behaviour. The observed development of the constraint norm $||\Delta_{\mathcal{C}}||$ and the pseudodifference norm $||\Delta_{\mathcal{P}}||$ is described using the following notation:

$-/+$: The norm is smaller/greater than that of the unextended system in the whole domain of time integration.

$\uparrow$ / $\downarrow$: The norm is smaller/greater than that of the unextended system after small integration times and greater/smaller at the end of the integration.

The parameter choices for the run 1 were based on our expectations explained in section II. With this choice we were able to reduce the growth of the violation of constraints, but we neither made the constraint submanifold an attractor nor did we improve the pseudodifference at the end of the evolution. Since we observed that the variables λ grew faster and to larger values than we had expected, we added terms proportional to λ^2 (run 2–4), to increase the damping for non-vanishing λs. We did not observe any significant change in the behaviour. This may have two reasons: Either the additional damping is too weak, a change in the parameters **D** and **E** alone is not sufficient, or these parameters are not the appropriate slots. To obtain a better understanding of the effect of the single parameters we performed the numerical experiments 5–19 whose results we are going to discuss in the following subsections.

B Influence of the parameter B

In the experiments 5–7, we studied the influence of the parameter **B** setting **B** proportional to the unit matrix, $\mathbf{B} = b\,\underline{\underline{1}}$, and varying b. The matrix **E** equals the unit matrix in all cases. The choice of the parameter b changes some of the characteristics of the λ-system. Absolute values of b greater than 1 imply that the λ-system has characteristic speeds larger than the speed of light. To avoid any influence of the grid boundary treatment on the numerical solution in the physical part of the grid — in the case $|b| > 1$ the outer grid boundary is no longer causally disconnected from the physical part of the grid — we moved the grid boundaries further out, something one can easily afford to do in a 1D calculation with moderate values b. For our purposes this was sufficient and we, therefore, did not discretise the analytic treatment of the initial boundary value problem for the λ-system which would guarantee that no constraint violation is fed in from the grid boundary. For $|b| > 1$ the maximally allowed time step is smaller than that of the unextended system due to the Courant-Friedrichs-Lewy condition. To compare numerical experiments for systems with different values b, we use the same, most restrictive time step for all runs.

For small values of b we do not observe a significant change in the behaviour of the λ-system compared to the unextended system, as can be seen in the FIG. 4 and 5. In these figures we plot the constraint norm (7) and the pseudodifference norm (8) for $b = -1$ (dashed line) and for $b = 1.2$ (dotted line) in addition to the unextended system (solid line). The curves are very similar, as are all other curves from the runs summarised as run number 5 in TABLE I. There is a slightly reduced growth in the constraint norm and an increase in the pseudodifference norm at the end of the evolution.

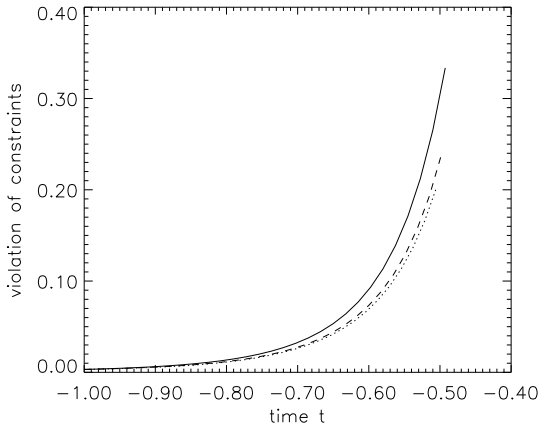

FIG. 4: Constraint norm $||\Delta_{\mathcal{C}}||(t)$ for the runs 5 with $b = -1$ (dashed line) and 6 (dotted line) in comparison to the unextended system (solid line).

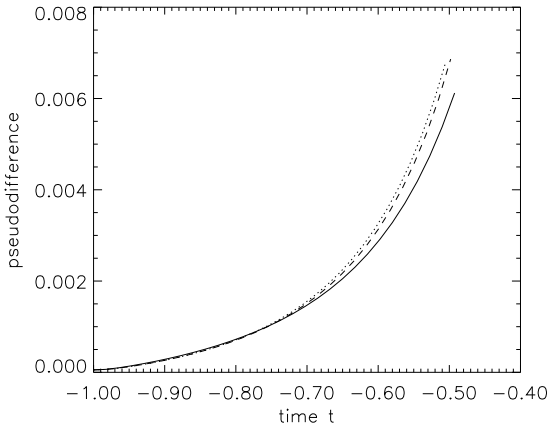

FIG. 5: Pseudodifference norm $||\Delta_{\mathcal{P}}||(t)$ for the runs 5 with $b = -1$ (dashed line) and 6 (dotted line) in comparison to the unextended system (solid line).

For a value of b significantly greater than 1 (run 7 and FIG. 2 and 3) the constraint norm decreases initially and is always smaller than in the unextended system. In contrast, as already mentioned, the pseudodifference norm is always larger than in the unextended system.

C Influence of the parameter E

In runs 8-14 we studied the role of the parameter $\mathbf{E}$, fixing the value of $\mathbf{B}$ to $\mathbf{B} = \underline{\underline{1}}$. A non-zero value of $\mathbf{B}$ is indeed necessary if λ is to measure the violation of the constraints. We choose the value $\mathbf{B} = \underline{\underline{1}}$, as the characteristic speeds determined by $\mathbf{B}$ then agree with speed of light which seems to be a natural choice for the field equations of general relativity. In addition, the results in the previous subsection were rather insensitive to the exact value of the parameter $\mathbf{B}$ in this part of the parameter space. Changing the value of diagonal elements for a constant diagonal matrix $\mathbf{E}$ in experiments 8-11, we found the best results for the violation of the constraints and the pseudodifference for a value of $\mathbf{E} = -3\ \underline{\underline{1}}$ (FIG. 6 and FIG. 7), where the variables λ are amplified by the $\mathbf{E}\lambda$-term in the λ-system. With this choice of parameters, the pseudodifference norm can be slightly improved during the whole numerical integration up to $t = -0.5$, but we stress that this improvement is not significant. We checked the results for this run after a longer integration time (up to $t = -0.3$). We then found a worse pseudodifference norm compared to the unextended system. In runs 12-14 we put only single diagonal elements of $\mathbf{E}$ to -3, $(\mathbf{E})_{11}$ and $(\mathbf{E})_{88}$, which influence directly those two constraints which are most vehemently violated. These constraints are the constraints for the quantities h_{11} and E_{11}. Only affecting both constraints with our choice of parameters can improve the numerical evolution of the constraints and the pseudodifference compared to the unextended system. However, in comparison to run 10, the results are worse.

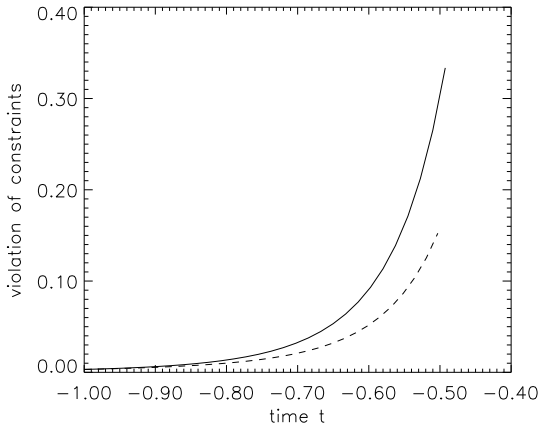

FIG. 6: Constraint norm $||\Delta_{\mathcal{C}}||(t)$ for run 10 in comparison to the unextended system (solid line).

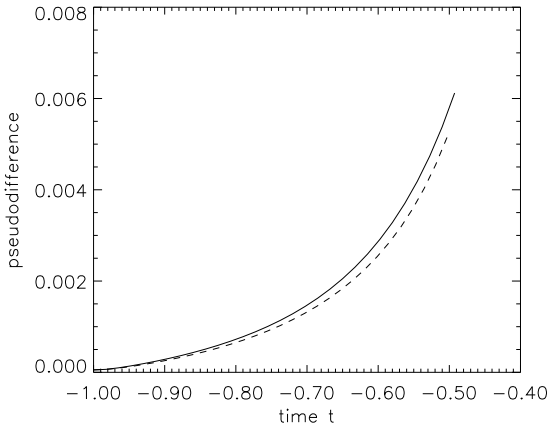

FIG. 7: Pseudodifference norm $||\Delta_{\mathcal{P}}||(t)$ for run 10 in comparison to the unextended system (solid line).

D Influence of the parameter D

With the experiment 15, we studied the influence of a constant, diagonal matrix $\mathbf{D}$ together with a matrix $\mathbf{B} = \underline{\underline{1}}$. In all runs with non-vanishing $\mathbf{D}$ the violation of constraints could be improved (see e.g. FIG. 8 for $d = 10$) at the cost of a worse pseudodifference. The constraint and the pseudodifference norm are identical for runs with $\mathbf{D} = d\ \underline{\underline{1}}$ and $\mathbf{D} = -d\ \underline{\underline{1}}$. This property results from a symmetry of all time evolution variables in (3) under the simultaneous transition $\mathbf{D} \to -\mathbf{D}$, $x \to -x$ for this specific choice of parameters. For the A3-solution, all evolution variables at a fixed time are even/odd functions on the space coordinate x. For a diagonal, constant matrix $\mathbf{D}$, the term $\mathbf{D}\lambda$ couples to an even/odd function f_i the corresponding λ_i, which has, according to (3c), the opposite symmetry, as it measures the corresponding constraint, which involves one space derivative of f_i.

E Influence of the parameter C

In the experiments with a non-vanishing matrix $\mathbf{C}$ (run 16) the violation of the constraints was only improved at the cost of a worse pseudodifference. As the result for the constraint norm is similar to that in FIG. 8, and the result for the pseudodifference norm is qualitatively given by FIG. 3, we refrain from presenting figures for run 16.

F Influence of the parameters D and E

Motivated by the good results for the pseudodifference in run 10 and for the constraints in run 15, we studied the correspondence of non-vanishing, diagonal parameters $\mathbf{D}$ and $\mathbf{E}$ for a parameter $\mathbf{B} = \underline{\underline{1}}$ in runs 17-19. Using the same parameters $\mathbf{B}, \mathbf{C}$ and $\mathbf{E}$ as in run 10, but

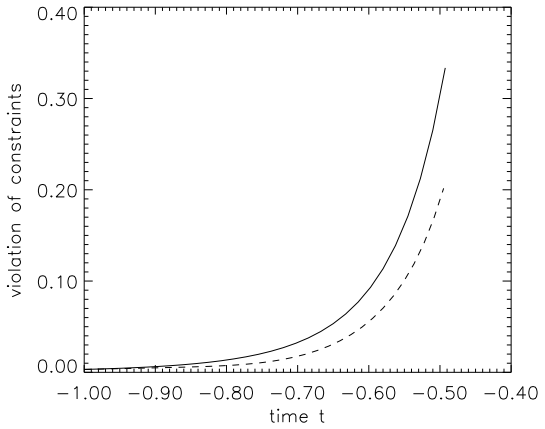

FIG. 8: Constraint norm $||\Delta_{\mathcal{C}}||(t)$ for run 15 with $d = 10$ in comparison to the unextended system (solid line).

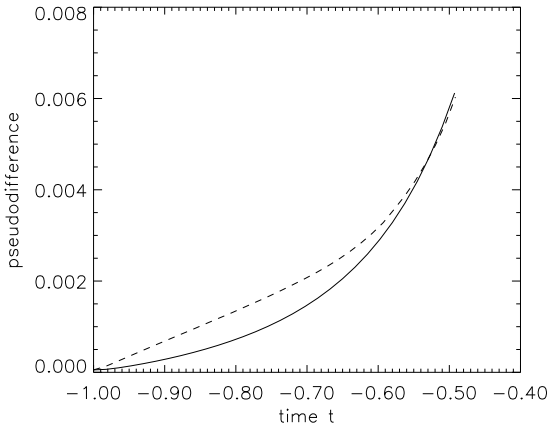

FIG. 9: Pseudodifference norm $||\Delta_{\mathcal{P}}||(t)$ for run 19 in comparison to the unextended system (solid line).

now with a non-vanishing $\mathbf{D}$, we could not improve the numerical solution in run 17. Hence, in runs 18-19, we again stuck to our original choice of $\mathbf{E} = \underline{\underline{1}}$. In run 18, the pseudodifference first increased, before approaching the curve of the unextended system at integration times of about $t = -0.5$ (FIG. 9). In experiment 19, we chose the matrix $\mathbf{D} = 5x\ \underline{\underline{1}}$ in order to keep the symmetries of the A3 solution. Again, the constraints were only improved at the cost of a worse solution.

V. CONCLUSION AND OUTLOOK

The freedom in extending a system of evolution equations with constraints to a λ-system is huge. For the conformal field equations of general relativity, we have explored the effect of what we thought are natural choices in the λ-system, analysing the influence on the quality of the new system's numerical solution. We found that we were able to significantly reduce the violation of the constraints, but we also found that this improvement did not imply a smaller numerical error.

Furthermore, we found that the significant improvement in the violation of the constraint did not prevent the solution from eventually running away from the constraint submanifold, i.e. the λ-systems used do not inherit the property of asymptotic stability from the linear system. Similar experience with the semi-linear SU(2)-Yang-Mills equations [11] and the study of a simplified model system [12] suggest that a more balanced choice of parameters of the λ-system is needed to achieve an attractive force towards the constraint submanifold for all times. Recent analytic results by Heinz-Otto Kreiss and Peter Hübner give sufficient conditions for asymptotic stability [in preparation]. It remains to be seen whether asymptotic stability implies a smaller numerical error.

ACKNOWLEDGEMENT

We would like to thank B. Schmidt and O. Brodbeck for helpful discussions. Peter Hübner would also like to thank the Albert-Einstein-Institut in Golm for supporting the writing of the code described in [7] and most of the work described in this paper by providing a postdoc position. Florian Siebel thanks the members of the Albert-Einstein-Institut for the support during his Diplomarbeit.

REFERENCES

[1] Brodbeck O., Frittelli S., Hübner P., Reula O., *J. Math. Phys.* **40** (1999) 909-923.
[2] Choptuik M.W., *Phys. Rev. D* **44** (1991) 3124-3135.
[3] Detweiler S., *Phys. Rev. D* **35** (1987) 1095-1099.
[4] Friedrich H., *Proc. R. Soc. London A* **375** (1981) 169-184.
[5] Friedrich H., *Proc. R. Soc. London A* **378** (1981) 401-421.
[6] Friedrich H., *Commun. Math. Phys.* **91** (1983) 445-472.
[7] Hübner P., *Class. Quantum Grav.* **16** (1999) 2145-2164.
[8] Hübner P., *Class. Quantum Grav.* **15** (1998) L21-L25.
[9] Hübner P., *Class. Quantum Grav.* **16** (1999) 2823-2843.
[10] Lax P.D., Wendroff B., *Comm. Pure Appl. Math.* **17** (1964) 381.
[11] Brodbeck O., Hübner P., unpublished work.
[12] Siebel F., *Diploma thesis* LMU Munich (1999).